

Geophysical Research Letters

RESEARCH LETTER

10.1002/2017GL073116

Key Points:

- Electron butterfly distributions occur more frequently at the geomagnetically active times than at the quite times
- A positive relation between magnetosonic waves and electron butterfly distributions
- No close relation between whistler-mode waves and electron butterfly distributions

Supporting Information:

- Supporting Information S1
- Text S1
- Figure S1
- Figure S2
- Figure S3
- Figure S4
- Figure S5
- Figure S6
- Figure S7
- Figure S8
- Figure S9
- Figure S10
- Figure S11
- Figure S12

Correspondence to:

Z. Su,
szpe@mail.ustc.edu.cn

Citation:

Yang, C., et al. (2017), A positive correlation between energetic electron butterfly distributions and magnetosonic waves in the radiation belt slot region, *Geophys. Res. Lett.*, 44, 3980–3990, doi:10.1002/2017GL073116.

Received 17 FEB 2017

Accepted 25 MAR 2017

Accepted article online 29 MAR 2017

Published online 14 MAY 2017

A positive correlation between energetic electron butterfly distributions and magnetosonic waves in the radiation belt slot region

Chang Yang^{1,2} , Zhenpeng Su^{1,3} , Fuliang Xiao² , Huinan Zheng^{1,3} , Yuming Wang^{1,3} , Shui Wang^{1,3}, H. E. Spence⁴ , G. D. Reeves^{5,6} , D. N. Baker⁷ , J. B. Blake⁸ , and H. O. Funsten⁹ 

¹Department of Geophysics and Planetary Sciences, University of Science and Technology of China, Hefei, China, ²School of Physics and Electronic Sciences, Changsha University of Science and Technology, Changsha, China, ³Collaborative Innovation Center of Astronautical Science and Technology, University of Science and Technology of China, Hefei, China,

⁴Institute for the Study of Earth, Oceans, and Space, University of New Hampshire, Durham, New Hampshire, USA, ⁵Space Science and Applications Group, Los Alamos National Laboratory, Los Alamos, New Mexico, USA, ⁶Space Sciences Division, The New Mexico Consortium, Los Alamos, New Mexico, USA, ⁷Laboratory for Atmospheric and Space Physics, University of Colorado Boulder, Boulder, Colorado, USA, ⁸Aerospace Corporation, Los Angeles, California, USA, ⁹ISR Division, Los Alamos National Laboratory, Los Alamos, New Mexico, USA

Abstract Energetic (hundreds of keV) electrons in the radiation belt slot region have been found to exhibit the butterfly pitch angle distributions. Resonant interactions with magnetosonic and whistler-mode waves are two potential mechanisms for the formation of these peculiar distributions. Here we perform a statistical study of energetic electron pitch angle distribution characteristics measured by Van Allen Probes in the slot region during a 3 year period from May 2013 to May 2016. Our results show that electron butterfly distributions are closely related to magnetosonic waves rather than to whistler-mode waves. Both electron butterfly distributions and magnetosonic waves occur more frequently at the geomagnetically active times than at the quiet times. In a statistical sense, more distinct butterfly distributions usually correspond to magnetosonic waves with larger amplitudes and vice versa. The averaged magnetosonic wave amplitude is less than 5 pT in the case of normal and flat-top distributions with a butterfly index BI = 1 but reaches ~50–95 pT in the case of distinct butterfly distributions with BI > 1.3. For magnetosonic waves with amplitudes >50 pT, the occurrence rate of butterfly distribution is above 80%. Our study suggests that energetic electron butterfly distributions in the slot region are primarily caused by magnetosonic waves.

1. Introduction

The Van Allen radiation belts are normally two zones of energetic particles separated by the slot region. In contrast to the relatively stable inner belt protons, the outer radiation belt electrons often exhibit dramatic variations [e.g., Baker *et al.*, 1986, 2013; Li *et al.*, 2001; Reeves *et al.*, 2003, 2013; Su *et al.*, 2014a, 2016; Anderson *et al.*, 2015; Ni *et al.*, 2015a, 2016a]. Outer radiation belt electrons can penetrate significantly into the slot region during the geomagnetic storms [Li *et al.*, 2001], and these slot electrons experience a slow decay during the quiescent period [Lyons and Thorne, 1973; Thorne *et al.*, 2013a; He *et al.*, 2016].

One of the important indicators of radiation belt dynamics is the particle pitch angle distribution pattern. In particular, the formation and flattening of butterfly pitch angle distributions (with a minimum around 90°) have attracted much attention. At the nightside large *L* shell region, the butterfly distributions of electrons with energies from ~100 keV to several MeV can frequently occur [Gannon *et al.*, 2007; Gu *et al.*, 2011; Ni *et al.*, 2015a, 2016b; Yu *et al.*, 2016], primarily due to adiabatic transport [Su *et al.*, 2010, 2011a; Kim *et al.*, 2010], drift-shell splitting [Sibeck *et al.*, 1987; Selesnick and Blake, 2002], and magnetopause shadowing [Hudson *et al.*, 2014]. The rapid flattening of butterfly distributions at energies from hundreds of keV to several MeV on a timescale of several hours has been interpreted as a consequence of chorus-driven local acceleration [Horne *et al.*, 2003; Yang *et al.*, 2016]. Recently, the butterfly distributions of electrons with energies of hundreds of keV have been found to occur at the low *L* shell regions (inner belt and slot region) [Zhao *et al.*, 2014a, 2014b], which are considered a result of resonant interactions with magnetosonic waves

[Horne et al., 2007; Xiao et al., 2015a; Li et al., 2016a] or whistler-mode waves (plasmaspheric hiss, lightning-generated whistlers, and very low frequency transmitters) [Albert et al., 2016]. For the former mechanism, the energy diffusion by magnetosonic waves can produce the electron distributions peaking at intermediate pitch angles [Horne et al., 2007]. For the latter mechanism, the cross diffusion is expected to cause the peaks of distributions away from 90° [Albert et al., 2016]. In this letter, to determine the dominant mechanism for the formation of butterfly distributions, we present a statistical study of energetic electron pitch angle distributions and magnetosonic/whistler-mode waves observed by Van Allen Probes over a 3 year period (from May 2013 to May 2016) in the radiation belt slot region.

2. Methods

The electron differential fluxes j were measured by Magnetic Electron Ion Spectrometer (MagEIS) instrument [Blake et al., 2013] of Energetic Particle, Composition, and Thermal Plasma (ECT) suite [Spence et al., 2013]. The time resolution of Level 3 data is ~ 11 s, and we smooth the data over ~ 33 s. We introduce the butterfly index $BI = \max\{j(\alpha)/j(\alpha = 90^\circ)\}$ [Yang et al., 2016] to quantitatively describe the local pitch angle α distribution pattern. The butterfly index BI equals 1 for normal or flat-top distributions, and a larger BI corresponds to a more distinct butterfly distribution. There are some minor differences between the electron energy channels of the MagEIS instruments on board Van Allen Probes A and B, for example, the counterpart of the energy channel 232 keV of the Probe A is 242 keV of the Probe B. We therefore combine the similar energy channels of Van Allen Probes A and B to obtain more data for the statistics.

The wave spectra were detected by Waveform Receiver instrument of Electric and Magnetic Field Instrument Suite and Integrated Science (EMFISIS) suite [Kletzing et al., 2013]. The singular value decomposition technique [Santolik et al., 2003] is used to calculate the wave ellipticity and normal angle. The magnetosonic wave, with a frequency range between the proton gyrofrequency f_{cp} and the lower hybrid frequency f_{LHR} , usually has an ellipticity close to 0 and a propagation direction nearly perpendicular to the background magnetic field [Santolik et al., 2002, 2004; Ma et al., 2013, 2016]. The following criteria are used to identify the magnetosonic waves: (1) the wave frequency lies in the range between the proton gyrofrequency f_{cp} and the lower hybrid frequency f_{LHR} , (2) the absolute value of wave ellipticity is less than 0.2, and (3) the wave normal angle is larger than 80°. In the slot region, the whistler-mode waves mainly include plasmaspheric hiss with a frequency range from tens to hundreds of Hertz and lightning-generated whistlers with frequencies around several kHz [Abel and Thorne, 1998; Meredith et al., 2007]. These whistler-mode waves are right-hand polarized, and the wave normal angles are generally less than 60° [Dunckel and Helliwell, 1969; Thorne et al., 1973; Li et al., 2013, 2015a]. The criteria for the identification of whistler-mode waves are specified as follows: (1) the wave frequency is larger than the proton gyrofrequency f_{cp} ($f_{cp} \approx 30$ Hz at $L = 2.5$), (2) the wave ellipticity is larger than 0.5, and (3) the wave normal angle lies between 0° and 60°. The wave amplitude B_t is defined as

$$B_t = \sqrt{\sum_i P_B^i \times \Delta f^i} \quad (1)$$

where i denotes the frequency band with the width Δf^i (in unit of Hz) and the power spectral density P_B^i (in unit of nT²/Hz), and the summation is performed over the frequency bands meeting the previously described criteria.

3. Correlated Data and Statistical Analysis

Figure 1 shows a 1 day overview of geomagnetic indices, plasma waves, and energetic electron local pitch angle distributions in the slot region. On 27 August 2015, a moderate geomagnetic storm was triggered with a minimum $Dst \approx -91$ nT and strong substorm activities occurred with a maximum $AE \approx 1800$ nT (Figure 1a). When the spacecraft passed through $L = 2.5$ (Figures 1b–1d), whistler-mode waves can be always observed but intense magnetosonic waves occurred only around 07:58 UT and 17:00 UT. Corresponding to the intense magnetosonic waves, energetic electrons clearly exhibited the butterfly distributions (Figures 1f and 1h). However, in the absence of distinct magnetosonic waves, energetic electrons displayed the normal or flat-top distributions at 00:27 UT (Figure 1e) and 09:29 UT (Figure 1g).

Figure 2 plots the butterfly index BI for indicated energy channels as a function of magnetic local time (MLT) and magnetic latitude (MLAT) at $L = 2.5$ during the 3 year period. The electron butterfly index is found to be nearly independent of MLT probably because energetic electrons experience an azimuthal drift around the

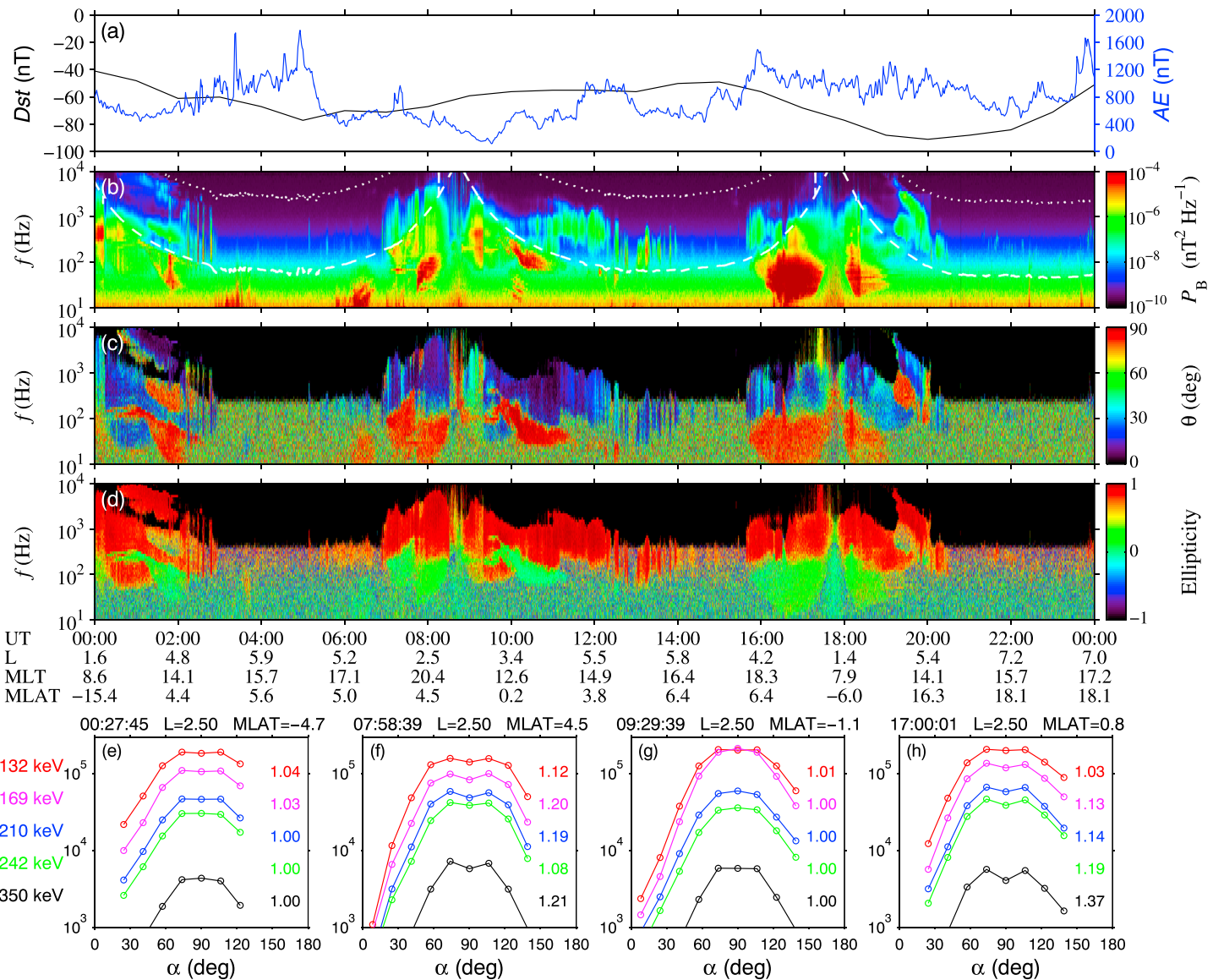


Figure 1. (a) Geomagnetic indices Dst (black) and AE (blue) during 27 August 2015. (b) Magnetic field wave spectra in the frequency range of 10–10000 Hz measured by Van Allen Probe B, overplotted with the electron gyrofrequencies f_{ce} (dotted) and the lower hybrid frequencies f_{LHR} (dashed). (c) Wave normal angle, and (d) ellipticity. (e–h) Electron differential fluxes (color coded according to energy) at selected times with the butterfly indices labeled in the panels.

Earth. However, the butterfly distributions with $BI > 1$ appear to be confined near the equator, which may be explained by the fact that the observed butterfly distributions usually peak around the equatorial pitch angles $|\alpha_{eq} - 90^\circ| = 16^\circ$ (Figures 1f and 1h). The electrons with $|\alpha_{eq} - 90^\circ| < 16^\circ$ are trapped within the magnetic latitudes $\lambda < 7.5^\circ$, and the local pitch angle distributions at $\lambda > 7.5^\circ$ are more likely to obey the normal or flat-top distributions. Consequently, considering that magnetosonic waves stay primarily close to equator within a few degrees of latitude [Santolik et al., 2004; Horne et al., 2007; Ma et al., 2013], we focus on those nearly equatorial events (with $\lambda < 3^\circ$) of both waves and electrons.

Figure 3 presents the histograms of magnetosonic and whistler-mode wave amplitudes B_t at $L = 2.5$ as functions of geomagnetic indices Dst and AE . Clearly, there is a positive correlation between magnetosonic wave amplitude and geomagnetic activity strength. During geomagnetic quiet times ($Dst > -20$ nT), the averaged magnetosonic wave amplitude is very small ($B_t < 5$ pT). The magnetosonic wave amplitude increases to $B_t \approx 20$ pT for small storms (-50 nT $< Dst < -30$ nT) and reaches $B_t = 50 \sim 100$ pT for moderate or strong storms ($Dst < -50$ nT). Similarly, $B_t < 10$ pT for $AE < 400$ nT but $B_t \approx 60$ pT for $AE \approx 1000$ nT. The results above

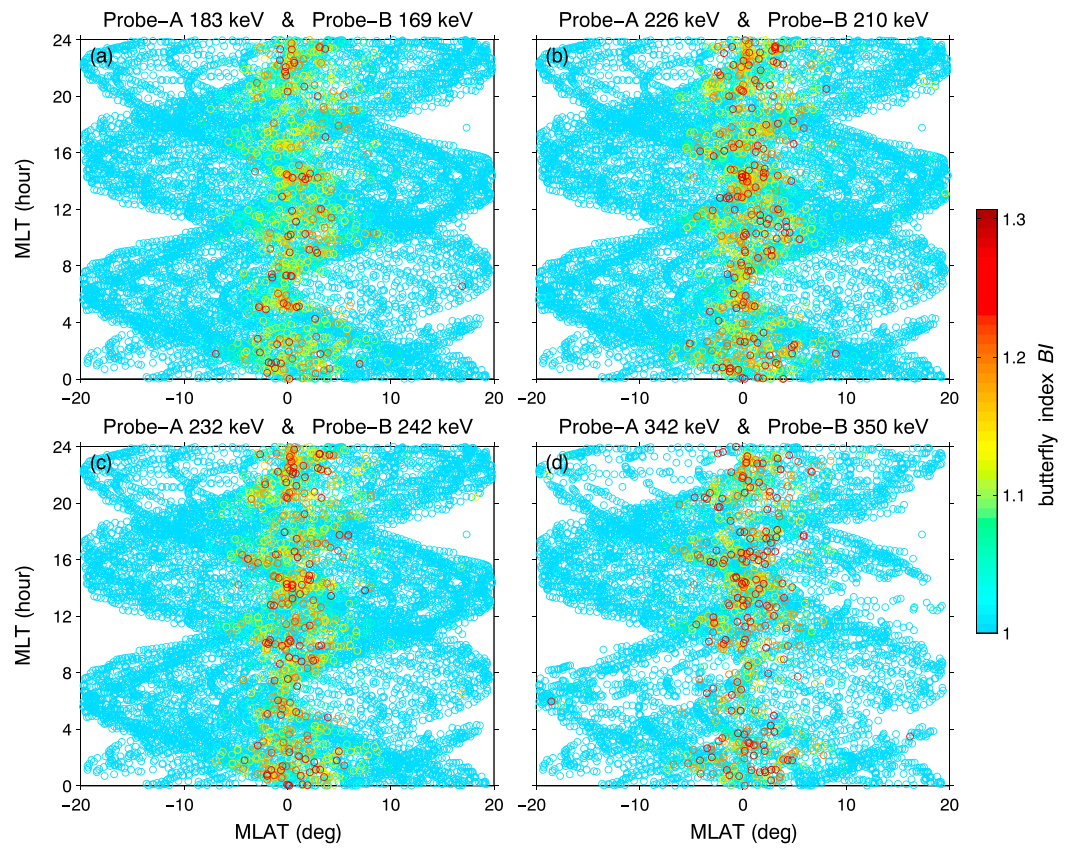


Figure 2. Butterfly index BI (color coded) as a function of MLT and MLAT at $L = 2.5$. Four panels correspond to four groups of energy channels, respectively.

are reasonable because magnetosonic waves are generated by a ring distribution of ~ 10 keV energetic protons injected from the plasmasheet into the inner magnetosphere [Meredith *et al.*, 2008; Gary *et al.*, 2010]. During high geomagnetic activities, such proton injection becomes larger under the drive of enhanced plasma convection, leading to higher magnetosonic wave growth [Chen *et al.*, 2010a, 2010b; Xiao *et al.*, 2012, 2013, 2015b; Ma *et al.*, 2016]. In contrast, the correlation between whistler-mode wave amplitude in the slot region and geomagnetic activity strength becomes relatively poor. The average wave amplitude peaks in the range $30 \text{ pT} < B_t < 50 \text{ pT}$ and exhibits minor variations when $AE < 800 \text{ nT}$. The averaged wave amplitude is about 20 pT during quiet times and increases to 40 pT during strong substorms ($AE > 800 \text{ nT}$), roughly comparable to the previous statistical results [Meredith *et al.*, 2007]. At $L = 2.5$, the whistler-mode wave power is mainly provided by the plasmaspheric hiss. The statistical behavior of whistler-mode wave amplitude may

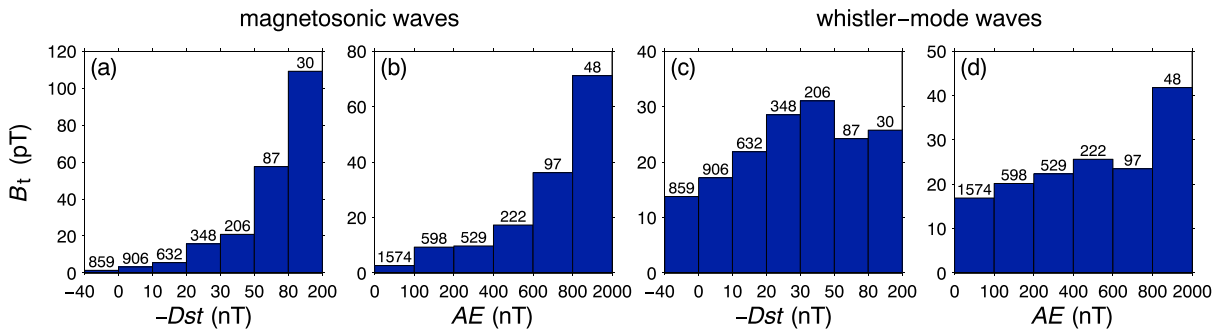


Figure 3. Histograms of (a and b) magnetosonic wave and (c and d) whistler-mode wave amplitude B_t as functions of geomagnetic indices Dst and AE at $L = 2.5$. The sample numbers are labeled above the histograms.

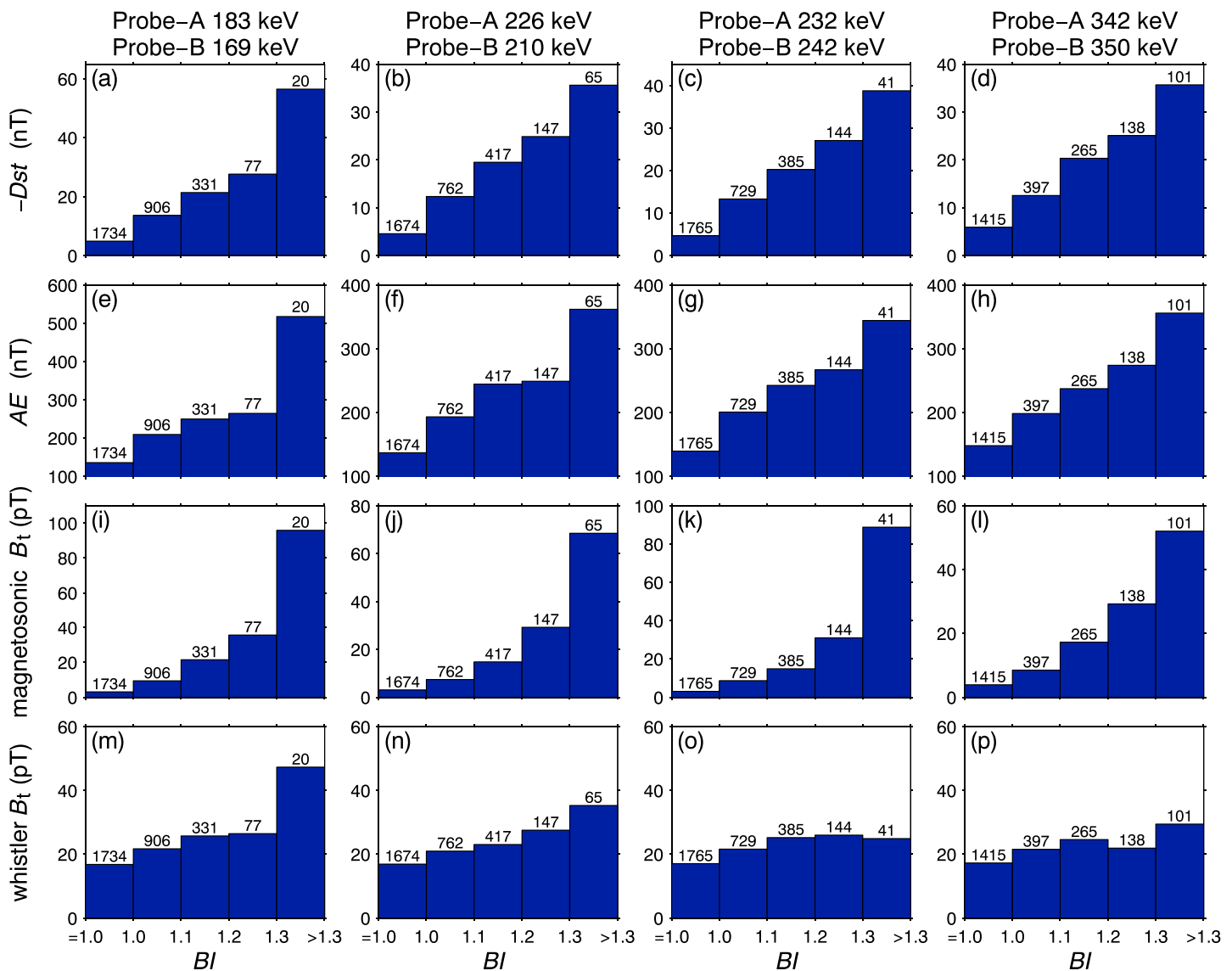


Figure 4. Histograms of geomagnetic indices (a–d) Dst , (e–h) AE , (i–l) magnetosonic wave amplitude B_t , and (m–p) whistler-mode wave amplitude B_t as functions of butterfly index BI at $L = 2.5$. The sample numbers in each BI range are labeled above the histograms.

be caused by the combination of external source and internal instability [Bortnik *et al.*, 2008, 2009; Chen *et al.*, 2012; Li *et al.*, 2015b; Su *et al.*, 2015a; Liu *et al.*, 2017]. Regardless of substorms or not, the dayside chorus can serve as the external source of plasmaspheric hiss [Liu *et al.*, 2017]. However, the amplification of hiss waves is favorable under the condition of strong substorm injections [Chen *et al.*, 2012].

Figure 4 gives the histograms of geomagnetic indices and wave amplitudes as functions of butterfly index for the indicated energy channels at $L = 2.5$. Larger BI events correspond to larger values of $-Dst$ and AE , indicating that more distinct butterfly distributions occur during higher geomagnetic activities. For all the four groups of energy channels, there is a positive correlation between BI and magnetosonic wave B_t . The averaged magnetosonic wave amplitude B_t is less than 5 pT for the normal or flat-top distributions with BI = 1.0 and stays in the range 50–95 pT (depending on the energy channel) for the distinct butterfly distributions with BI > 1.3 . At the first two groups of energy channels 169–226 keV, BI weakly correlates with whistler-mode B_t . As BI increases from 1.0 to 1.3, whistler-mode wave B_t increases by about 2 times. For the other two groups of energy channels 232–350 keV, BI and whistler-mode wave B_t appear to be independent of each other. No matter how large BI is, the averaged whistler-mode wave B_t keeps to be ~ 20 pT. In order to further show

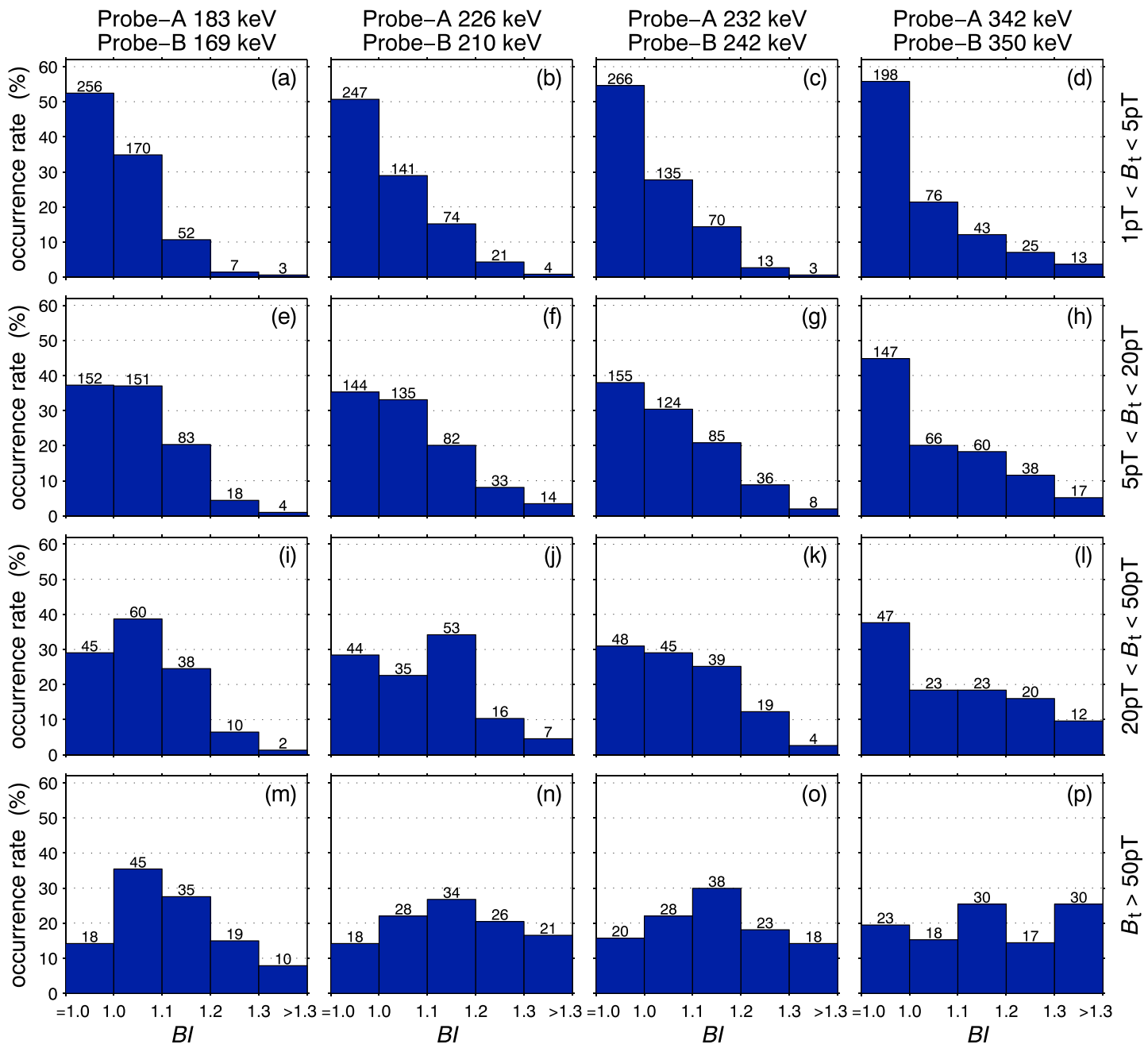


Figure 5. Histograms of the occurrence rates of different electron distributions as functions of magnetosonic wave amplitude B_t at $L = 2.5$.

the correlation between butterfly distributions and waves, we present the scatterplots of butterfly indices as functions of magnetosonic and whistler-mode wave amplitude B_t (Figures S1 and S2 in the supporting information) and the histograms of butterfly indices as functions of magnetosonic wave amplitude, whistler-mode wave amplitude, and their ratio (Figure S3) in the supporting information. All these observations suggest that the butterfly distributions in the slot region are more closely related with magnetosonic waves than whistler-mode waves.

Figures 5 and 6 display the occurrence rates of different pitch angle distributions at different levels of wave strength at $L = 2.5$. In each panel, the occurrence rate is defined by event number in each BI range divided by the total number for all BI under the given condition of wave amplitude. Clearly, the occurrence rate of butterfly distributions with $BI > 1$ increases with the increasing magnetosonic wave amplitude B_t (Figure 5).

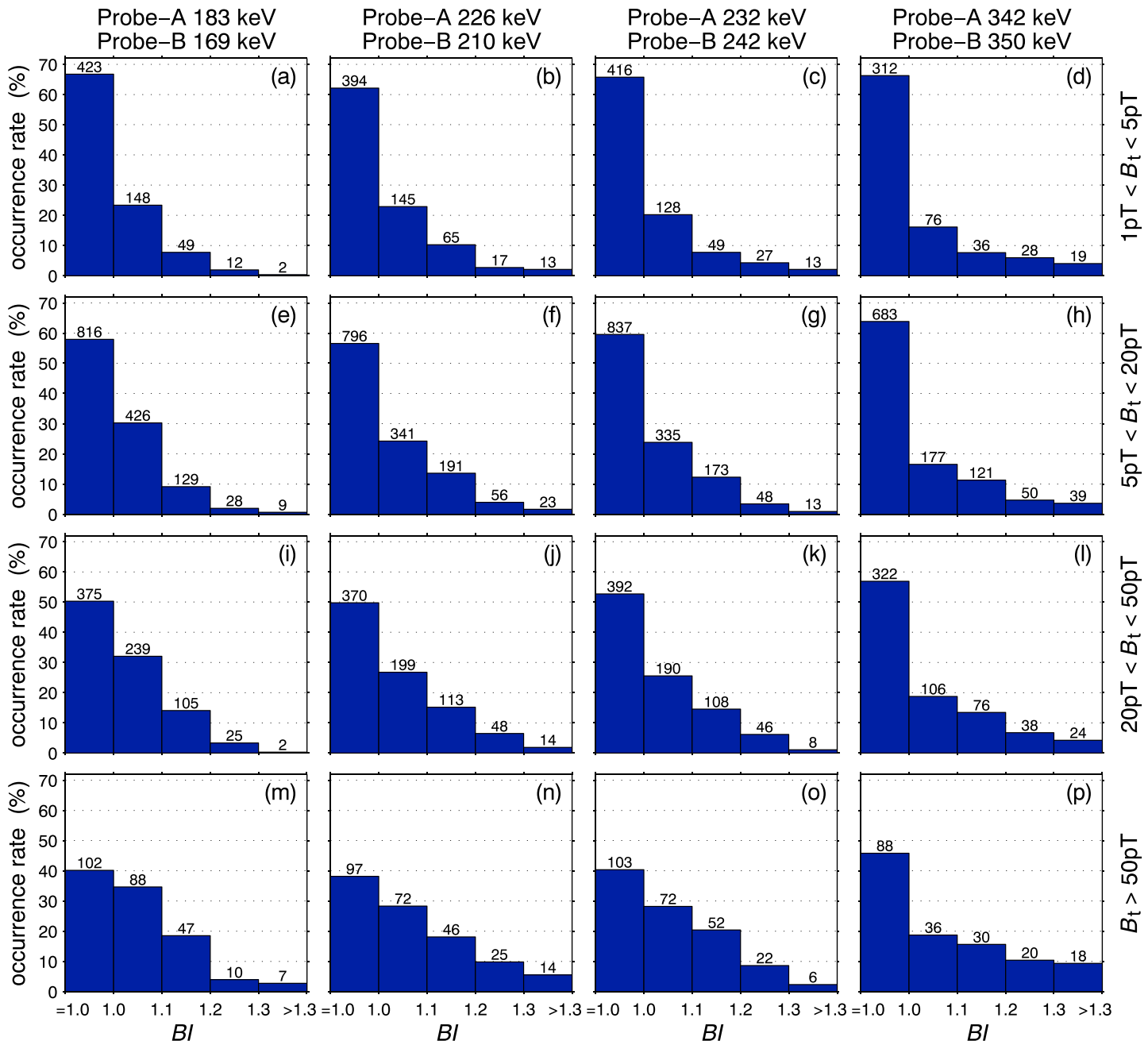


Figure 6. Same as Figure 5 except for whistler-mode wave amplitude B_t .

In the case of weak magnetosonic waves ($1 \text{ pT} < B_t < 5 \text{ pT}$), the occurrence rate is approximately 40%–50% for butterfly distributions with $BI > 1$. For strong magnetosonic waves with $B_t > 50 \text{ pT}$, the occurrence rate of butterfly distributions reaches >80%. As magnetosonic wave amplitude B_t increases from the range 1–5 pT to the range >50 pT, the occurrence rate of distinct butterfly distributions with $BI > 1.3$ increases from the range 2–5% to the range 8–28% (depending on energy channels). In contrast, the enhancement of whistler-mode waves cannot significantly increase the occurrence rate of butterfly distributions. Even for the large amplitude (>50 pT) whistler-mode waves, the occurrence rate of butterfly distributions lies in the range 50%–60%. As shown in Figure 5, electrons with higher energies tend to exhibit more distinct butterfly patterns (e.g., $BI > 1.3$) than those with lower energies, which can be reasonably explained by the energy dependence of Landau resonance between magnetosonic waves and electrons [Horne et al., 2007; Li et al., 2016a, 2016b].

As simulated by *Li et al.* [2016a], magnetosonic waves at $L = 2.4$ produce butterfly distributions most efficiently for $E_k = 467$ keV, and the efficiency gradually drops with the decrease of electron energy. For the electrons of $E_k < 100$ keV, magnetosonic waves are difficult to produce distinct butterfly distributions (with large BI). This is further confirmed by statistical results at lower energy channels (54–134 keV) (Figures S4–S6) in the supporting information. For the higher energy channels ($E_k \geq 467$ keV), due to the relatively poor integrity of the electron flux data, it is difficult to carry out a valid statistical analysis. These observations demonstrate once again the importance of magnetosonic waves for the generation of energetic electron butterfly distributions in the radiation belt slot region.

In the statistics above, we focus on the heart of the slot region $L = 2.5$, because it can basically reflect the whole slot region. We have also carried out some statistical analysis at $L = 2.0$ and 3.0 (Figures S7–S12) in the supporting information. Compared to the situation at $L = 2.5$, the butterfly distribution has a less (or more) chance to occur at $L = 3.0$ (or $L = 2.0$). The correlations between butterfly distributions and magnetosonic or whistler-mode waves at these L shells are similar to those at $L = 2.5$.

4. Conclusion and Discussion

Radiation belt electrons often exhibit significant variations [e.g., *Li et al.*, 2001; *Baker et al.*, 2013; *Su et al.*, 2014a, 2014b; *Reeves et al.*, 2016] due to various adiabatic [e.g., *Lyons*, 1977; *Kim and Chan*, 1997; *Su et al.*, 2010] and nonadiabatic [e.g., *Horne and Thorne*, 1998; *Summers et al.*, 1998; *Elkington et al.*, 1999; *Horne et al.*, 2005; *Shprits et al.*, 2006; *Omura et al.*, 2007; *Su et al.*, 2011b, 2015b; *Mann et al.*, 2013; *Thorne et al.*, 2013b; *Ni et al.*, 2015b; *Gao et al.*, 2016; *Wang et al.*, 2016] processes. Electron pitch angle distribution pattern is an important indicator of radiation belt dynamics. Recent observational studies have found the occurrence of butterfly pitch angle distributions of energetic (approximately hundreds of keV) electrons in the inner belt and slot region [*Zhao et al.*, 2014a, 2014b]. Two main plausible physical mechanisms for the formation of butterfly distributions at such low L shells are the resonant interactions with magnetosonic waves [*Horne et al.*, 2007; *Xiao et al.*, 2015a; *Li et al.*, 2016a] and whistler-mode waves [*Albert et al.*, 2016].

Using Van Allen Probes data from May 2013 to May 2016, we have statistically investigated the electron pitch angle distribution characteristics and plasma waves in the slot region. Butterfly distributions occur primarily near the equator (probably because the butterfly peaks usually lie around the equatorial pitch angles $|\alpha_{eq} - 90^\circ| = 16^\circ$) but display no preference for MLT (due to electron azimuthal drift around the Earth). The occurrence rate of energetic electron butterfly distribution is higher during the stronger geomagnetic storm and substorm activities. The amplitude of magnetosonic waves, as compared to whistler-mode waves, exhibits a more positive correlation with the strength of geomagnetic activities. In a statistical sense, more distinct butterfly distributions of all the energy channels (169–350 keV) usually correspond to larger-amplitude magnetosonic waves and vice versa. For the normal and flat-top distributions with a butterfly index $BI = 1$, the averaged magnetosonic wave amplitude is less than 5 pT. In contrast, for the distinct butterfly distributions with a butterfly index $BI > 1.3$, the averaged magnetosonic wave amplitude increases to 50–95 pT. As magnetosonic wave amplitude increases from 1–5 pT to >50 pT, the occurrence rate of distinct butterfly distribution with $BI > 1.3$ increases from 2–5% to 8–28% (depending on energy channels). Under the condition of large-amplitude (>50 pT) magnetosonic waves, the occurrence rate of butterfly distribution $BI > 1$ is above 80%. However, the correlation between butterfly index and whistler-mode wave amplitude appears to be quite weak. Even under the condition of large amplitude (>50 pT) whistler-mode waves, the occurrence rate of butterfly distribution lies in the range 50%–60%. Our study supports that Landau resonance with magnetosonic waves [*Horne et al.*, 2007; *Li et al.*, 2016a, 2016b] is a primary cause of energetic electron butterfly distributions in the slot region.

The whistler-mode waves (plasmaspheric hiss, lightning-generated whistlers, and very low frequency transmitters) are usually invoked to explain the gradual loss of energetic electrons in the slot region [e.g., *Lyons et al.*, 1972; *Abel and Thorne*, 1998; *Meredith et al.*, 2007]. In fact, the scattering of whistler-mode waves becomes quite weak for the near-equatorially trapped electrons [e.g., *Meredith et al.*, 2009; *He et al.*, 2016]. The Landau resonance with magnetosonic waves can act at the pitch angles $|\alpha - 90^\circ| < 20^\circ$ [*Horne et al.*, 2007; *Li et al.*, 2016a], probably affecting the energetic electron lifetime in the slot region particularly during the geomagnetically active periods. Hence, the magnetosonic waves should be taken into account in future radiation belt models.

Acknowledgments

This work was supported by the National Natural Science Foundation of China grants 41422405, 41631071, 41274174, 41174125, 41131065, 41421063, 41231066, and 41304134; the Chinese Academy of Sciences grants KZCX2-EW-QN510 and KZZD-EW-01-4; the CAS Key Research Program of Frontier Sciences grant QYZDB-SSW-DQC015; the National Key Basic Research Special Foundation of China grant 2011CB811403, and the Fundamental Research Funds for the Central Universities WK2080000077. We acknowledge J.H. King, N. Papatashvili, and CDAWeb for the use of magnetospheric indices and acknowledge the University of Iowa as the source for the EMFISIS data (this acknowledgement does not imply endorsement of the publication by the University of Iowa or its researchers). Data are available at the following websites: http://cdaweb.gsfc.nasa.gov/cdaweb/istp_public/ (geomagnetic activity indices), <http://emfisis.physics.uiowa.edu/Flight/> (EMFISIS), and http://www.rbsp-ect.lanl.gov/data_pub/ (ECT).

References

- Abel, B., and R. M. Thorne (1998), Electron scattering loss in Earth's inner magnetosphere: 1. Dominant physical processes, *J. Geophys. Res.*, **103**, 2385–2396, doi:10.1029/97JA02919.
- Albert, J. M., R. B. M. P. Starks, M. J. Horne, and S. A. Glaert (2016), Quasi-linear simulations of inner radiation belt electron pitch angle and energy distributions, *Geophys. Res. Lett.*, **43**, 2381–2388, doi:10.1002/2016GL067938.
- Anderson, B. R., R. M. Millan, G. D. Reeves, and R. H. W. Friedel (2015), Acceleration and loss of relativistic electrons during small geomagnetic storms, *Geophys. Res. Lett.*, **42**, 10,113–10,119, doi:10.1002/2015GL066376.
- Baker, D. N., R. W. Klebesadel, P. R. Higbie, and J. B. Blake (1986), Highly relativistic electrons in the Earth's outer magnetosphere. I. Lifetimes and temporal history 1979–1984, *J. Geophys. Res.*, **91**, 4265–4276, doi:10.1029/JA091iA04p04265.
- Baker, D. N., et al. (2013), A long-lived relativistic electron storage ring embedded in Earth's outer Van Allen belt, *Science*, **340**, 186–190, doi:10.1126/science.123518.
- Blake, J. B., et al. (2013), The magnetic electron ion spectrometer (MagEIS) instruments aboard the radiation belt storm probes (RBSP) spacecraft, *Space Sci. Rev.*, **179**, 383–421, doi:10.1007/s11214-013-9991-8.
- Bortnik, J., R. M. Thorne, and N. P. Meredith (2008), The unexpected origin of plasmaspheric hiss from discrete chorus emissions, *Nature*, **452**, 62–66, doi:10.1038/nature06741.
- Bortnik, J., W. Li, R. M. Thorne, V. Angelopoulos, C. Cully, J. Bonnell, O. Le Contel, and A. Roux (2009), An observation linking the origin of plasmaspheric hiss to discrete chorus emissions, *Science*, **324**, 775–778, doi:10.1126/science.1171273.
- Chen, L., R. M. Thorne, V. K. Jordanova, C. Wang, M. Gkioulidou, L. Lyons, and R. B. Horne (2010a), Global simulation of EMIC wave excitation during the 21 April 2001 storm from coupled RCM-RAM-HOTRAY modeling, *J. Geophys. Res.*, **115**, A07209, doi:10.1029/2009JA015075.
- Chen, L., R. M. Thorne, V. K. Jordanova, and R. B. Horne (2010b), Global simulation of magnetosonic waves instability in the storm time magnetosphere, *J. Geophys. Res.*, **115**, A11222, doi:10.1029/2010JA015707.
- Chen, L., W. Li, J. Bortnik, and R. M. Thorne (2012), Amplification of whistler-mode hiss inside the plasmasphere, *Geophys. Res. Lett.*, **39**, L08111, doi:10.1029/2012GL051488.
- Dunkel, N., and R. A. Helliwell (1969), Whistler-mode emissions on the OGO 1 satellite, *J. Geophys. Res.*, **74**, 6371–6385, doi:10.1029/JA074i026p06371.
- Elkington, S. R., M. K. Hudson, and A. A. Chan (1999), Acceleration of relativistic electrons via drift-resonant interaction with toroidal-mode PC-5 ULF oscillations, *Geophys. Res. Lett.*, **26**, 3273–3276, doi:10.1029/1999GL003659.
- Gannon, J. L., X. Li, and D. Heynderickx (2007), Pitch angle distribution analysis of radiation belt electrons based on combined release and radiation effects satellite medium electrons a data, *J. Geophys. Res.*, **112**, A05212, doi:10.1029/2005JA011565.
- Gao, Z., Z. Su, H. Zhu, F. Xiao, H. Zheng, Y. Wang, C. Shen, and S. Wang (2016), Intense low-frequency chorus waves observed by Van Allen Probes: Fine structures and potential effect on radiation belt electrons, *Geophys. Res. Lett.*, **43**, 967–977, doi:10.1002/2016GL067687.
- Gary, S. P., K. Liu, D. Winske, and R. E. Denton (2010), Ion Bernstein instability in the terrestrial magnetosphere: Linear dispersion theory, *J. Geophys. Res.*, **115**, A12209, doi:10.1029/2010JA015965.
- Gu, X., Z. Zhao, B. Ni, Y. Y. Shprits, and C. Zhou (2011), Statistical analysis of pitch angle distribution of radiation belt energetic electrons near the geostationary orbit: CRRES observations, *J. Geophys. Res.*, **116**, A01208, doi:10.1029/2010JA016052.
- He, Z., Q. Yan, Y. Chu, and Y. Cao (2016), Wave-driven gradual loss of energetic electrons in the slot region, *J. Geophys. Res. Space Physics*, **121**, 8614–8623, doi:10.1002/2016JA023087.
- Horne, R. B., and R. M. Thorne (1998), Potential waves for relativistic electron scattering and stochastic acceleration during magnetic storms, *Geophys. Res. Lett.*, **25**, 3011–3014, doi:10.1029/98GL01002.
- Horne, R. B., N. P. Meredith, R. M. Thorne, D. Heyndericks, R. H. A. Iles, and R. R. Anderson (2003), Evolution of energetic electron pitch angle distributions during storm time electron acceleration to megaelectronvolt energies, *J. Geophys. Res.*, **108**(A1), 1016, doi:10.1029/2001JA009165.
- Horne, R. B., et al. (2005), Wave acceleration of electrons in the Van Allen radiation belts, *Nature*, **437**, 227–230, doi:10.1038/nature03939.
- Horne, R. B., R. M. Thorne, S. A. Glaert, N. P. Meredith, D. Pokhotelov, and O. Santolík (2007), Electron acceleration in the Van Allen radiation belts by fast magnetosonic waves, *Geophys. Res. Lett.*, **34**, L17107, doi:10.1029/2007GL030267.
- Hudson, M. K., D. N. Baker, J. Goldstein, B. T. Kress, J. Paral, F. R. Toffoletto, and M. Wittherger (2014), Simulated magnetopause losses and Van Allen Probe flux dropouts, *Geophys. Res. Lett.*, **41**, 1113–1118, doi:10.1002/2014GL059222.
- Kim, H.-J., and A. A. Chan (1997), Fully adiabatic changes in storm time relativistic electron fluxes, *J. Geophys. Res.*, **102**, 22,107–22,116, doi:10.1029/97JA01814.
- Kim, K. C., D. Lee, H. Kim, E. S. Lee, and C. R. Choi (2010), Numerical estimates of drift loss and *Dst* effect for outer radiation belt relativistic electrons with arbitrary pitch angle, *J. Geophys. Res.*, **115**, A03208, doi:10.1029/2009JA014523.
- Kletzing, C. A., et al. (2013), The Electric and Magnetic Field Instrument Suite and Integrated Science (EMFISIS) on RBSP, *Space Sci. Rev.*, **179**, 127–181, doi:10.1007/s11214-013-9993-6.
- Li, J., et al. (2016a), Formation of energetic electron butterfly distributions by magnetosonic waves via Landau resonance, *Geophys. Res. Lett.*, **43**, 3009–3016, doi:10.1002/2016GL067853.
- Li, J., et al. (2016b), Ultrarelativistic electron butterfly distributions created by parallel acceleration due to magnetosonic waves, *J. Geophys. Res. Space Physics*, **121**, 3212–3222, doi:10.1002/2016JA022370.
- Li, W., et al. (2013), An unusual enhancement of low-frequency plasmaspheric hiss in the outer plasmasphere associated with substorm-injected electrons, *Geophys. Res. Lett.*, **40**, 3798–3803, doi:10.1002/grl.50787.
- Li, W., Q. Ma, R. M. Thorne, J. Bortnik, C. A. Kletzing, W. S. Kurth, G. B. Hospodarsky, and Y. Nishimura (2015a), Statistical properties of plasmaspheric hiss derived from Van Allen Probes data and their effects on radiation belt electron dynamics, *J. Geophys. Res. Space Physics*, **120**, 3393–3405, doi:10.1002/2015JA021048.
- Li, W., L. Chen, J. Bortnik, R. M. Thorne, V. Angelopoulos, C. A. Kletzing, W. S. Kurth, and G. B. Hospodarsky (2015b), First evidence for chorus at a large geocentric distance as a source of plasmaspheric hiss: Coordinated THEMIS and Van Allen Probes observation, *Geophys. Res. Lett.*, **42**, 241–248, doi:10.1002/2014GL062832.
- Li, X., D. N. Baker, S. G. Kanekal, M. Looper, and M. Temerin (2001), Long term measurements of radiation belts by SAMPEX and their variations, *Geophys. Res. Lett.*, **28**, 3827–3830, doi:10.1029/2001GL013586.
- Liu, N., et al. (2017), Simultaneous disappearances of plasmaspheric hiss, exohiss and chorus waves triggered by a sudden decrease in solar wind dynamic pressure, *Geophys. Res. Lett.*, **44**, 52–61, doi:10.1002/2016GL071987.
- Lyons, L. R. (1977), Adiabatic evolution of trapped particle pitch angle distributions during a storm main phase, *J. Geophys. Res.*, **82**, 2428–2432, doi:10.1029/JA082i016p02428.
- Lyons, L. R., and R. M. Thorne (1973), Equilibrium structure of radiation belt electrons, *J. Geophys. Res.*, **78**, 2142–2149, doi:10.1029/JA078i013p02142.

- Lyons, L. R., R. M. Thorne, and C. F. Kennel (1972), Pitch-angle diffusion of radiation belt electrons within the plasmasphere, *J. Geophys. Res.*, 77, 3455–3474.
- Ma, Q., W. Li, R. M. Thorne, and V. Angelopoulos (2013), Global distribution of equatorial magnetosonic waves observed by THEMIS, *Geophys. Res. Lett.*, 40, 1895–1901, doi:10.1002/grl.50434.
- Ma, Q., W. Li, R. M. Thorne, J. Bortnik, C. A. Kletzing, W. S. Kurth, and G. B. Hospodarsky (2016), Electron scattering by magnetosonic waves in the inner magnetosphere, *J. Geophys. Res. Space Physics*, 121, 274–285, doi:10.1002/2015JA021992.
- Mann, I. R., et al. (2013), Discovery of the action of a geophysical synchrotron in the Earth's Van Allen radiation belts, *Nat. Commun.*, 4, 2795, doi:10.1038/ncomms3795.
- Meredith, N. P., R. B. Horne, S. A. Glauert, and R. R. Anderson (2007), Slot region electron loss timescales due to plasmaspheric hiss and lightning-generated whistlers, *J. Geophys. Res.*, 112, A08214, doi:10.1029/2007JA012413.
- Meredith, N. P., R. B. Horne, and R. R. Anderson (2008), Survey of magnetosonic waves and proton ring distributions in the Earth's inner magnetosphere, *J. Geophys. Res.*, 113, A06213, doi:10.1029/2007JA012975.
- Meredith, N. P., R. B. Horne, S. A. Glauert, D. N. Baker, S. G. Kanekal, and J. M. Albert (2009), Relativistic electron loss timescales in the slot region, *J. Geophys. Res.*, 114, A03222, doi:10.1029/2008JA013899.
- Ni, B., et al. (2015a), Variability of the pitch angle distribution of radiation belt ultrarelativistic electrons during and following intense geomagnetic storms: Van Allen Probes observations, *J. Geophys. Res. Space Physics*, 120, 4863–4876, doi:10.1002/2015JA021065.
- Ni, B., et al. (2015b), Resonant scattering of outer zone relativistic electrons by multi-band EMIC waves and resultant electron loss timescales, *J. Geophys. Res. Space Physics*, 120, 7357–7373, doi:10.1002/2015JA021466.
- Ni, B., Z. Xiang, X. Gu, Y. Shprits, C. Zhou, Z. Zhao, X. Zhang, and P. Zuo (2016a), Dynamic responses of the Earth's radiation belts during periods of solar wind dynamic pressure pulse based on normalized superposed epoch analysis, *J. Geophys. Res. Space Physics*, 121, 8523–8536, doi:10.1002/2016JA023067.
- Ni, B., Z. Zou, X. Li, J. Bortnik, L. Xie, and X. Gu (2016b), Occurrence characteristics of outer zone relativistic electron butterfly distribution: A survey of Van Allen Probes REPT measurements, *Geophys. Res. Lett.*, 43, 5644–5652, doi:10.1002/2016GL069350.
- Omura, Y., N. Furuya, and D. Summers (2007), Relativistic turning acceleration of resonant electrons by coherent whistler mode waves in a dipole magnetic field, *J. Geophys. Res.*, 112, A06236, doi:10.1029/2006JA012243.
- Reeves, G. D., K. L. McAdams, R. H. W. Friedel, and T. P. O'Brien (2003), Acceleration and loss of relativistic electrons during geomagnetic storms, *Geophys. Res. Lett.*, 30(10), 1529, doi:10.1029/2002GL016513.
- Reeves, G. D., et al. (2013), Electron acceleration in the heart of the Van Allen radiation belts, *Science*, 341(6149), 991–994, doi:10.1126/science.1237743.
- Reeves, G. D., et al. (2016), Energy-dependent dynamics of keV to MeV electrons in the inner zone, outer zone, and slot regions, *J. Geophys. Res. Space Physics*, 121, 397–412, doi:10.1002/2015JA021569.
- Santolík, O., J. S. Pickett, D. A. Gurnett, M. Maksimovic, and N. Cornilleau-Wehrlin (2002), Spatiotemporal variability and propagation of equatorial noise observed by Cluster, *J. Geophys. Res.*, 107(A12), 1495, doi:10.1029/2001JA009159.
- Santolík, O., D. A. Gurnett, J. S. Pickett, M. Parrot, and N. Cornilleau-Wehrlin (2003), Spatio-temporal structure of storm-time chorus, *J. Geophys. Res.*, 108(A7), 1278, doi:10.1029/2002JA009791.
- Santolík, O., F. Němcová, K. Gerecová, E. Macúšová, Y. de Conchy, and N. Cornilleau-Wehrlin (2004), Systematic analysis of equatorial noise below the lower hybrid frequency, *Ann. Geophys.*, 22, 2587–2595, doi:10.5194/angeo-22-2587-2004.
- Selesnick, R. S., and J. B. Blake (2002), Relativistic electron drift shell splitting, *J. Geophys. Res.*, 107(A9), 1265, doi:10.1029/2001JA009179.
- Shprits, Y. Y., R. M. Thorne, R. Friedel, G. D. Reeves, J. Fennell, D. N. Baker, and S. G. Kanekal (2006), Outward radial diffusion driven by losses at magnetopause, *J. Geophys. Res.*, 111, A11214, doi:10.1029/2006JA011657.
- Sibeck, D. G., R. W. McEntire, A. T. Y. Lui, R. E. Lopez, and S. M. Krimigis (1987), Magnetic field drift shell splitting: Cause of unusual dayside particle pitch angle distributions during storms and substorms, *J. Geophys. Res.*, 92, 13,485–13,497, doi:10.1029/JA092iA12p13485.
- Spence, H. E., et al. (2013), Science goals and overview of the energetic particle, composition, and thermal plasma (ECT) suite on NASA's Radiation Belt Storm Probes (RBSP) mission, *Space Sci. Rev.*, 179, 311–336, doi:10.1007/s11214-013-0007-5.
- Su, Z., F. Xiao, H. Zheng, and S. Wang (2010), Combined radial diffusion and adiabatic transport of radiation belt electrons with arbitrary pitch-angles, *J. Geophys. Res.*, 115, A10249, doi:10.1029/2010JA015903.
- Su, Z., F. Xiao, H. Zheng, and S. Wang (2011a), Radiation belt electron dynamics driven by adiabatic transport, radial diffusion, and wave-particle interactions, *J. Geophys. Res.*, 116, A04205, doi:10.1029/2010JA016228.
- Su, Z., F. Xiao, H. Zheng, and S. Wang (2011b), CRRES observation and STEERB simulation of the 9 October 1990 electron radiation belt dropout event, *Geophys. Res. Lett.*, 38, L06106, doi:10.1029/2011GL046873.
- Su, Z., et al. (2014a), Nonstorm time dynamics of electron radiation belts observed by the Van Allen Probes, *Geophys. Res. Lett.*, 41, 229–235, doi:10.1002/2013GL058912.
- Su, Z., et al. (2014b), Quantifying the relative contributions of substorm injections and chorus waves to the rapid outward extension of electron radiation belt, *J. Geophys. Res. Space Physics*, 119, 10,023–10,040, doi:10.1002/2014JA020709.
- Su, Z., et al. (2015a), Disappearance of plasmaspheric hiss following interplanetary shock, *Geophys. Res. Lett.*, 42, 3129–3140, doi:10.1002/2015GL063906.
- Su, Z., et al. (2015b), Ultra-low-frequency wave-driven diffusion of radiation belt relativistic electrons, *Nat. Commun.*, 6, 10096, doi:10.1038/ncomms10096.
- Su, Z., et al. (2016), Nonstorm time dropout of radiation belt electron fluxes on 24 September 2013, *J. Geophys. Res. Space Physics*, 121, 6400–6416, doi:10.1002/2016JA022546.
- Summers, D., R. M. Thorne, and F. Xiao (1998), Relativistic theory of wave-particle resonant diffusion with application to electron acceleration in the magnetosphere, *J. Geophys. Res.*, 103, 20,487–20,500, doi:10.1029/98JA01740.
- Thorne, R. M., E. J. Smith, R. K. Burton, and R. E. Holzer (1973), Plasmaspheric hiss, *J. Geophys. Res.*, 78, 1581–1596, doi:10.1029/JA078i010p01581.
- Thorne, R. M., et al. (2013a), Evolution and slow decay of an unusual narrow ring of relativistic electrons near $L \sim 3.2$ following the September 2012 magnetic storm, *Geophys. Res. Lett.*, 40, 3507–3511, doi:10.1002/grl.50627.
- Thorne, R. M., et al. (2013b), Rapid local acceleration of relativistic radiation-belt electrons by magnetospheric chorus, *Nature*, 504, 411–414, doi:10.1038/nature12889.
- Wang, B., Z. Su, Y. Zhang, S. Shi, and G. Wang (2016), Nonlinear Landau resonant scattering of near-equatorially mirroring radiation belt electrons by oblique EMIC waves, *Geophys. Res. Lett.*, 43, 3628–3636, doi:10.1002/2016GL068467.
- Xiao, F., Q. Zhou, Z. He, and L. Tang (2012), Three-dimensional ray tracing of fast magnetosonic waves, *J. Geophys. Res.*, 117, A06208, doi:10.1029/2012JA017589.

- Xiao, F., Q. Zhou, Z. He, C. Yang, Y. He, and L. Tang (2013), Magnetosonic wave instability by proton ring distributions: Simultaneous data and modeling, *J. Geophys. Res. Space Physics*, **118**, 4053–4058, doi:10.1002/jgra.50401.
- Xiao, F., C. Yang, Z. Su, Q. Zhou, Z. He, Y. He, D. Baker, H. Spence, H. Funsten, and J. Blake (2015a), Wave-driven butterfly distribution of Van Allen belt relativistic electrons, *Nat. Commun.*, **6**, 8590, doi:10.1038/ncomms9590.
- Xiao, F., Q. Zhou, Y. He, C. Yang, S. Liu, D. N. Baker, H. E. Spence, G. D. Reeves, H. Funsten, and J. Blake (2015b), Penetration of magnetosonic waves into the plasmasphere observed by the Van Allen Probes, *Geophys. Res. Lett.*, **42**, 7287–7294, doi:10.1002/2015GL065745.
- Yang, C., et al. (2016), Rapid flattening of butterfly pitch angle distributions of radiation belt electrons by whistler-mode chorus, *Geophys. Res. Lett.*, **43**, 8339–8347, doi:10.1002/2016GL070194.
- Yu, J., L. Li, J. B. Cao, G. D. Reeves, D. N. Baker, and H. Spence (2016), The influences of solar wind pressure and interplanetary magnetic field on global magnetic field and outer radiation belt electrons, *Geophys. Res. Lett.*, **43**, 7319–7327, doi:10.1002/2016GL069029.
- Zhao, H., X. Li, J. B. Blake, J. F. Fennell, S. G. Claudepierre, D. N. Baker, A. N. Jaynes, D. M. Malaspina, and S. G. Kanekal (2014a), Peculiar pitch angle distribution of relativistic electrons in the inner radiation belt and slot region, *Geophys. Res. Lett.*, **41**, 2250–2257, doi:10.1002/2014GL059725.
- Zhao, H., X. Li, J. B. Blake, J. F. Fennell, S. G. Claudepierre, D. N. Baker, A. N. Jaynes, and D. M. Malaspina (2014b), Characteristics of pitch angle distributions of hundreds of keV electrons in the slot region and inner radiation belt, *J. Geophys. Res. Space Physics*, **119**, 9543–9557, doi:10.1002/2014JA020386.